

CHEMISTRY

A European Journal

A Journal of



Accepted Article

Title: Thermotropic MIDA boronates as a case study for the role of dipolar interactions in liquid crystalline self-assembly

Authors: Tobias Wöhrle, Rafet Gündemir, Wolfgang Frey, Friederike Knecht, Andreas Köhn, and Sabine Laschat

This manuscript has been accepted after peer review and appears as an Accepted Article online prior to editing, proofing, and formal publication of the final Version of Record (VoR). This work is currently citable by using the Digital Object Identifier (DOI) given below. The VoR will be published online in Early View as soon as possible and may be different to this Accepted Article as a result of editing. Readers should obtain the VoR from the journal website shown below when it is published to ensure accuracy of information. The authors are responsible for the content of this Accepted Article.

To be cited as: *Chem. Eur. J.* 10.1002/chem.201605648

Link to VoR: <http://dx.doi.org/10.1002/chem.201605648>

Supported by
ACES

WILEY-VCH

Thermotropic MIDA boronates as a case study for the role of dipolar interactions in liquid crystalline self-assembly

Tobias Wöhrle,^a Rafet Gündemir,^a Wolfgang Frey,^a Friedericke Knecht,^b Andreas Köhn,^{c,*}
Sabine Laschat^{a,*}

^a Institut für Organische Chemie, Universität Stuttgart, Pfaffenwaldring 55, D-70569 Stuttgart,
Germany

E-mail: sabine.laschat@oc.uni-stuttgart.de

^b Institut für Physikalische Chemie, Universität Stuttgart, Pfaffenwaldring 55, D-70569 Stuttgart,
Germany

^c Institut für Theoretische Chemie, Universität Stuttgart, Pfaffenwaldring 55, D-70569 Stuttgart,
Germany

Abstract

A series of MIDA (N-methylimino diacetic acid) boronates carrying 4-alkoxy, 3,4-bisalkoxy, or 3,4,5-trisalkoxyphenyl substituents were synthesized and their mesomorphic properties characterized by differential scanning calorimetry (DSC), polarizing optical microscopy (POM) and X-ray diffraction (WAXS, SAXS). Most derivatives were liquid crystalline. In the case of mono- and bisalkoxy-substituted derivatives, already C₆ chains induced SmA mesophases despite the bulky MIDA head group. With increasing chain lengths Col_h phases replaced SmA phases in the disubstituted series. Quantum chemical calculations of a series of MIDA boronates show that the B-N bond is a dative bond with a positive charge on the boron atom and negative charges on the nitrogen and oxygen atoms, respectively. In addition, no π -interaction between aryl moiety and B-N bond was found, thus the mesogenic unit is electronically fully decoupled from the MIDA head group. These theoretical findings were supported by IR and Raman spectra and a single crystal structure analysis of 4-ethoxyphenyl MIDA boronate. Calculations of the electrostatic potential of the MIDA boronate reveal a special polarity pattern that can support the formation of a two-dimensional network and is likely to explain the liquid crystalline self-assembly. The absence of

any electronic cross talk between MIDA head group and B-aryl or B-alkyl substituents allows the efficient tailoring of the mesophase type through variation of the substituents.

Key words: MIDA, Boronate, Liquid Crystal, Smectic, Columnar, Quantum Chemical Calculation

Accepted Manuscript

Introduction

Boron containing materials have received increasing interest during the last decade due to their specific properties. For example, tris-coordinated boron compounds are Lewis acidic, isoelectronic with carbeniumions, possess π electron acceptor as well as inductive σ electron donor capacity, undergo formation of tetracoordinate borates and conjugate adjacent π -systems, while compounds containing B-N bonds are isoelectronic with the corresponding C-C analogues and display strong luminescence.^[1-7] With regard to thermotropic liquid crystals most work has been devoted to borondifluoride β -diketonates (or β -enaminoketonates),^[8-14] borondipyrrromethene (BODIPY) derivatives (**1**)^[15-27] and boron clusters (**2**)^[28-35] (Fig. 1). In diketonate and BODIPY derivatives such as **1** or subphthalocyanines, the boron atom is surrounded by a flat mesogenic π -system, which not only contributes to the liquid crystalline self-assembly, but also adds favorable absorption and emission characteristics. In contrast, the bulky *closo*-carboranes **2** are incorporated into rigid rod-like units in order to obtain suitable mesomorphic properties. These boron clusters are not only suitable for liquid crystal display applications due to their high dielectric anisotropy $\Delta\epsilon$ ^[31,36,37] but also as battery electrolytes.^[38] Moreover, they provided insight into fundamental aspects of soft matter such as the contribution of Coulomb and dipolar interactions on the stabilization of mesophases.^[7,32]

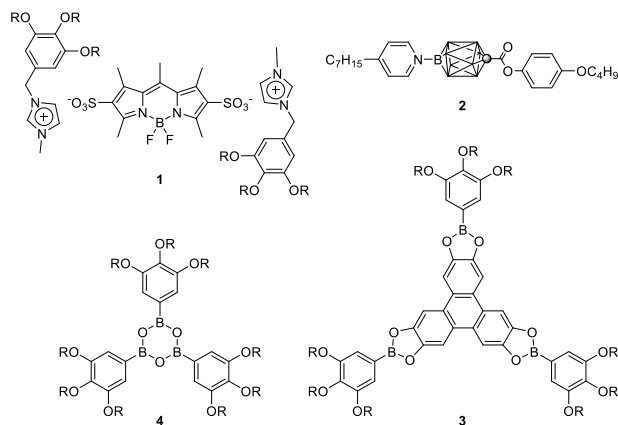


Figure 1. Discotic BODIPY **1**^[21], calamitic boron cluster **2**^[32], discotic borolane **3**^[48] and boroxine **4**^[49]

In contrast, boronic acids, boronates and derivatives thereof are much less explored regarding liquid crystalline properties despite their extensive use as highly versatile building blocks for transition metal-catalyzed cross-coupling reactions.^[39-42] Based on early work by Seto^[43-47]

electron deficient discotic triphenylene borolanes **3** have been developed by King.^[48] During our previous studies on discotic boroxines **4**^[49,50] we noticed that neither of the synthetic precursors, i.e. pinacol borolanes **5**^[51,52], boronic acids **6**^[49] and diethanolamine boronates **7** respectively, displayed any mesomorphism despite their wedge shape in case of 3,4,5-trisalkoxy-substituted derivatives and the possibility to enforce nanosegregation through hydrogen bonding for the latter two cases **6** and **7** (Fig. 2). In agreement with our own work a literature survey revealed that boronate derivatives **5** – **7** with only two or one side chain were not liquid crystalline.^[53-55,48,56] Much to our surprise the tetragonal *N*-methyliminodiacetic acid (MIDA) boronates **8** showed double melting, which was taken as evidence for mesophase formation.

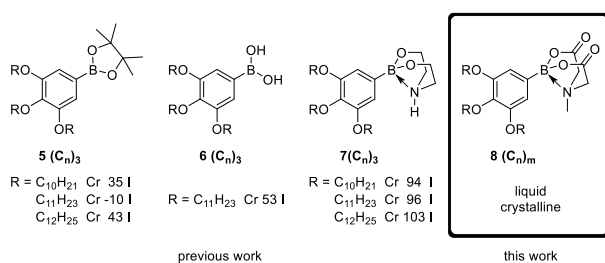


Figure 2. Pinacol borolanes **5** (C_n)₃ with $n = 10 - 12$ ^[51,52], boronic acid **6** (C_{11})_n^[49] and diethanolamin boronates **7** (C_n)₃ with $n = 10 - 12$ showing no liquid crystalline behaviour and liquid crystalline MIDA-boronates **8** (C_n)_m ($n = 6 - 14$, $m = 1 - 3$) presented in this work.

MIDA boronates are air stable Lewis acid/base complexes pioneered by Contreras^[57,58] and Burke^[59] as organoboron species, which are protected against transmetallation and can be reactivated for further cross coupling by simple saponification giving access to a great diversity of compound classes.^[60] Based on variable temperature NMR studies Contreras calculated an activation enthalpy of >90 kJ/mol for the cleavage of the B-N dative bond,^[57] indicating the remarkable stability. Further insight came from experimental and theoretical vibrational spectroscopy studies by Tschumper, Hemmer and coworkers.^[61] However, liquid crystalline self-assembly of MIDA boronates has not been reported in the literature.

For the formation of thermotropic liquid crystalline phases several factors are important. For example space filling, i.e. minimization of free volume, and shape anisotropy of the mesogenic molecules, i.e. disk- or rod-shaped mesogens with attached hydrophobic alkyl chains, are parameters, which lead to nanosegregation because structurally or chemically incompatible parts

do not mix with each other but occupy different domains.^[62-70] Other parameters such as π - π -interactions, hydrogen bonds or fluorophobic interactions also contribute to the stability of the mesophase.^[62-70] For example, hydrogen bonding determines the phase behaviour of supramolecular liquid crystal dimers as reported by Imrie.^[71] In addition, dimer formation of molecular dipoles has been identified as the origin for the reentrant behaviour of 4-alkoxy- and 4-alkyl-4-cyanobiphenyl binary mixtures.^[72] Polar interactions play a stabilizing role in bent-core molecules.^[73] For amphiphilic, ionic or zwitterionic liquid crystals nanosegregation of charged molecular subunits and less polar groups together with electrostatic interactions are the major driving forces for mesophase formation. Besides chemical incompatibility the difference in molecular flexibility contributes to nanosegregation.^[74] It should be emphasized that the presence of mesogenic units is not required in order to obtain liquid crystalline phases.^[74a] Prominent examples are lyotropic,^[75,76] amphotropic^[77] and ionic liquid crystals.^[66-70,78] As demonstrated by Saito, even classical thermotropic systems such as 4-alkylcyanobiphenyls display amphiphilic properties upon mixing with *n*-alkanes.^[77]

However, these various parameters did not provide an obvious explanation for the unique liquid crystalline self-assembly of MIDA boronates **8** with respect to boronic acid derivatives **5** – **7**. The above-mentioned lack of knowledge on the materials properties of MIDA boronates **8** motivated us to explore them as a novel class of thermotropic liquid crystals. Our aim was to understand the different phase behaviour of MIDA boronates **8** as compared to boronic acid derivatives **5** – **7**. By a combined theoretical and experimental study, we hoped to gain insight into the role of dipolar interactions on the liquid crystalline self-assembly of such Lewis acid/base complexes and to obtain design principles useful for other thermotropic liquid crystals. The results are described below.

Results and Discussion

Synthesis

Three series of MIDA boronates **8** (C_n), **8** (C_n)₂ and **8** (C_n)₃ (*n* = 4, 6, 8, 10, 12, 14) with one, two or three alkoxy side chains at the phenyl ring were prepared (Figure 3). Mono-, di- and trisalkoxybromobenzenes **9** – **11** were lithiated with *n*-BuLi, followed by sequential treatment with boron triisopropyl borate and MIDA according to the method by Burke^[79] and the resulting MIDA boronates **8** (C_n)_m were isolated in 20 - 75 % yield. For comparison, biphenyl derivative **13** (C_{12})

carrying a typical calamitic mesogenic subunit was prepared from the respective 4'-bromo-4-dodecoxy-biphenyl **12** accordingly.

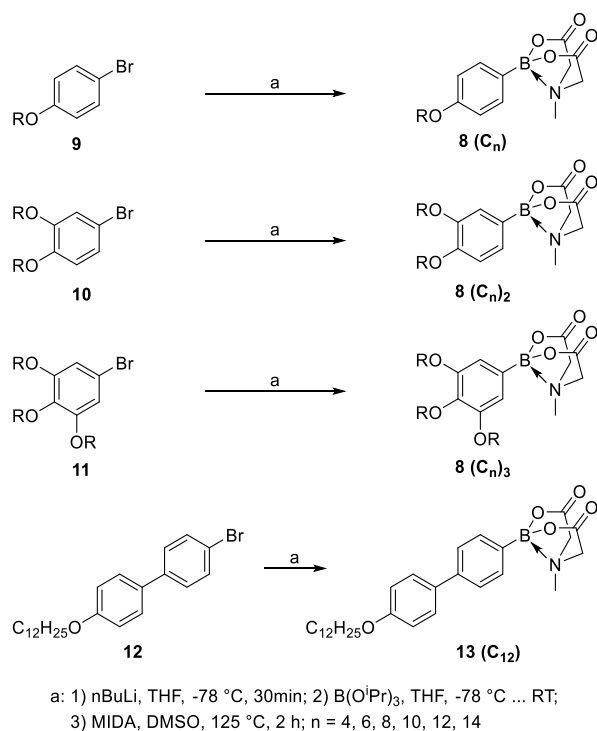


Figure 3. Synthesis of MIDA boronates **8** (C_n)_m and **13** (C_{12}).

Mesophase Behaviour

Mesomorphic properties were investigated by differential scanning calorimetry (DSC), polarizing optical microscopy (POM) and X-ray diffraction (WAXS, SAXS). A typical DSC curve is shown in Figure 4a for decyloxyphenyl MIDA boronate **8** (C_{10}). Upon 1st heating two endothermic phase transitions were visible, the melting from the crystalline to the liquid crystalline at $111\text{ }^\circ\text{C}$ and the clearing into the isotropic liquid at $178\text{ }^\circ\text{C}$. Upon 1st cooling only the formation of the liquid crystalline phase at $179\text{ }^\circ\text{C}$ was observed. Upon 2nd heating and 2nd cooling only the clearing points were observable. Due to the fact, that melting (or crystallization) peaks could not be clearly identified for most of the MIDA boronates, these transitions were determined via POM. For this purpose, the respective sample was heated and cooled with the same rates as in the DSC experiments ($\Delta = 5\text{K}\cdot\text{min}^{-1}$). If a phase transition occurred, heating and cooling was reiterated in that temperature range with lower heating and cooling rates ($\Delta = 2\text{K}\cdot\text{min}^{-1}$).

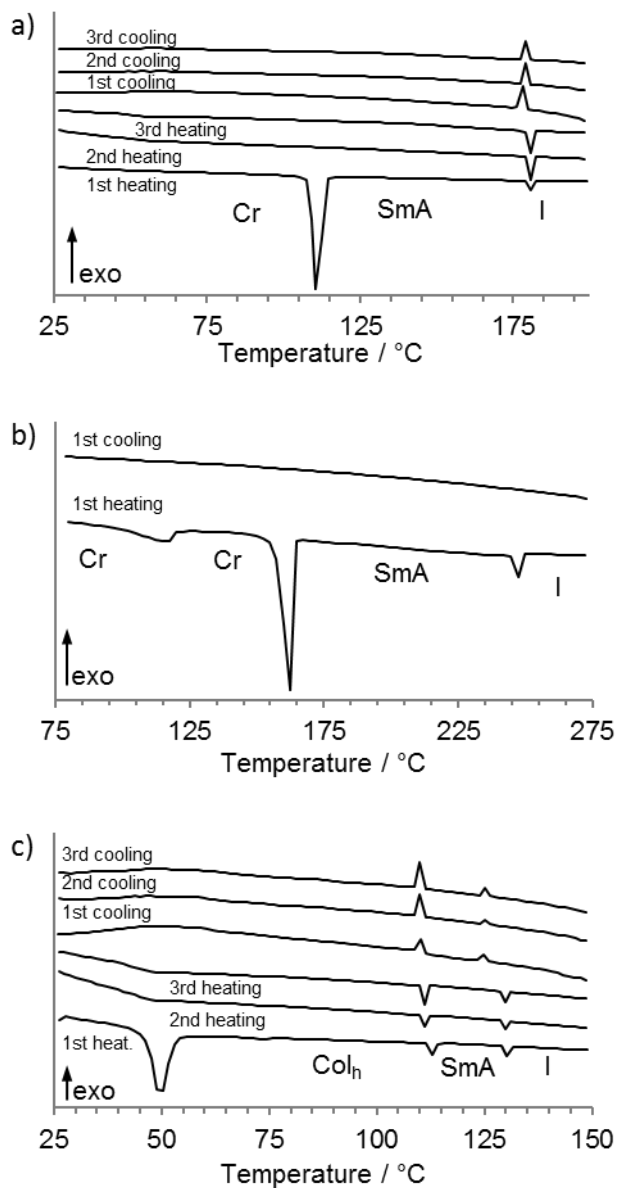


Figure 4. a) DSC traces of first, second and third heating / cooling cycle of **8** (C_{10}), b) DSC traces of first heating and cooling of **13** (C_{12}) (heating / cooling rate $5 \text{ K}\cdot\text{min}^{-1}$), c) DSC traces of first, second and third heating / cooling cycle of **8** (C_{10})₂ (heating / cooling rate $5 \text{ K}\cdot\text{min}^{-1}$).

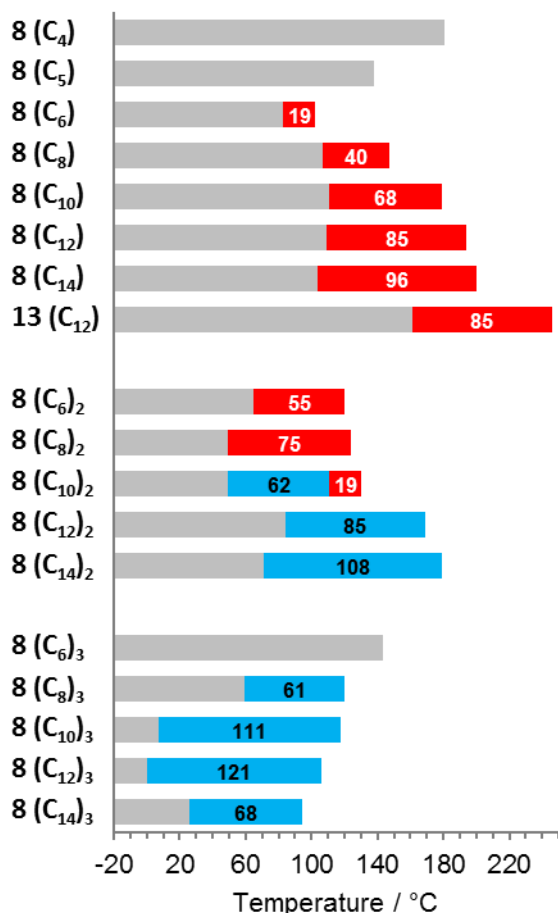


Figure 5. Phase widths of the MIDA boronates **8** (C_n)_m and **13** (C₁₂) obtained by DSC and POM (heating/cooling rate 5 K/min). Phase transition temperatures were taken upon second heating, exceptions: **8** (C₆) was taken upon second cooling, **13** (C₁₂) was taken upon first heating. The following phases were observed: ■ crystalline (Cr), ■ smectic A (SmA), ■ hexagonal columnar (Col_h).

The complementary DSC and POM results are summarized in Figure 5 (for details of DSC traces see Supp. Info). Compounds **8** (C₄), **8** (C₅), and **8** (C₆)₃ with short side chains were non-mesomorphic. All other MIDA boronates showed enantiotropic mesomorphism regardless of the number and lengths of side chains. For the monoalkoxyphenyl series **8** (C_n) mesophase widths and stabilities increased with increasing chain lengths *n* from 19 K (*n* = 6) to 96 K (*n* = 14). In order to check, whether the high clearing temperatures between 179 °C for **8** (C₁₀) and 200 °C for **6** (C₁₄) might lead to decomposition, TGA measurements for **8** (C₁₀) were carried out. As shown in Figure S18b, TGA revealed that the compound was stable up to 300 °C. For comparison, the mono-

substituted biphenyl **13** (**C**₁₂) was studied by DSC (Fig. 4b). Upon 1st heating three endothermic transitions were observed, at 116 °C a melting transition from crystalline to crystalline phase, at 161 °C to the liquid crystalline phase, and at 246 °C from the mesophase to the isotropic liquid. The phase width of 85 K is similar to the respective alkoxyphenyl derivative **8** (**C**₁₂), although, at elevated temperatures. During subsequent cooling no more phase transitions were visible. Presumably, clearing to the isotropic liquid lead to decomposition, which is in contrast to the thermal stability of the alkoxyphenyl derivative **8** (**C**₁₀). Under the POM strong homeotropic alignment was detected for the **8** (**C**_n) series and for **13** (**C**₁₂). After shearing filament-like textures were visible, suggesting the presence of a SmA phase (Figure 6). Presumably, homeotropic alignment is enforced by the polar head group interacting with the glass surface.

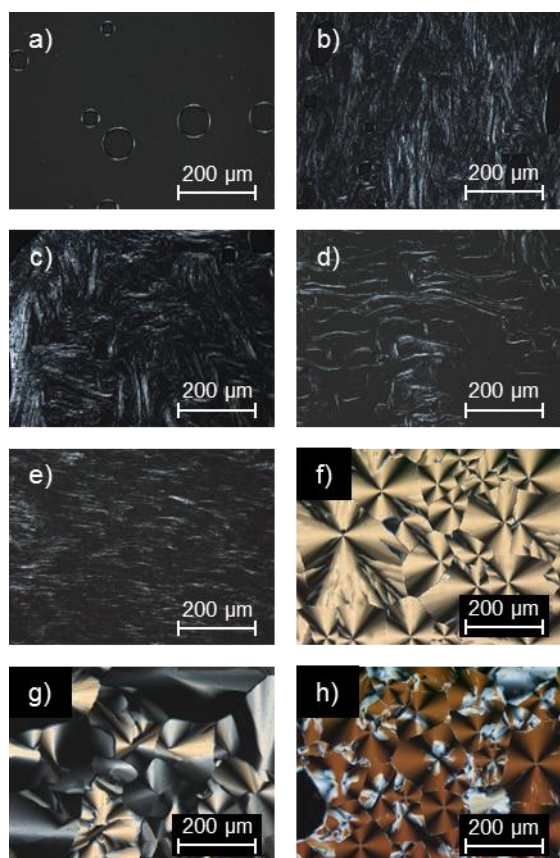


Figure 6. POM images: a) homeotropic aligned sample of **8** (**C**₁₀) at 170 °C, b) same sample of **8** (**C**₁₀) after shearing at 170 °C, c) **8** (**C**₁₂) after shearing at 150 °C, d) **13** (**C**₁₂) after shearing at 200 °C, e) **8** (**C**₁₀)₂ after shearing at 120 °C, f) **8** (**C**₁₀)₂ at 100 °C after cooling from the SmA phase, g) **8** (**C**₁₀)₃ at 105 °C, h) **8** (**C**₁₂)₃ at 100 °C. All images were taken during 2nd cooling from the isotropic liquid (except **13** (**C**₁₂))

which was investigated during 1st heating), heating/cooling rate was 5 K·min⁻¹, 100x magnification.

DSC and POM experiments of the dialkoxyphenyl series **8** (C_n)₂ showed in each case mesophases of similar phase widths as compared to the monoalkoxyphenyl series **8** (C_n), albeit decreased melting and clearing points. With increasing chain lengths n the clearing temperatures increased. More importantly, the phase type changed with increasing chain lengths. While the shortest member of the series **8** (C₆)₂ displayed a crystalline to SmA transition at 65°C and a clearing transition at 120°C upon heating, the higher homologue **8** (C₁₀)₂ displayed a melting point at 49°C, followed by a transition to the SmA phase at 111°C and a clearing transition at 130°C. The phase sequence is reproducible as can be seen in Figure 4c, however the melting point from crystalline state to the low temperature mesophase is broadened significantly during cooling and not visible in the 2nd and 3rd heating cycles. Under the POM **8** (C₆)₂ and **8** (C₈)₂ displayed strong homeotropic alignment with filament like textures after shearing. This indicates the presence of a SmA mesophase. The high temperature phase of **8** (C₁₀)₂ showed a similar behaviour implying a SmA phase as well (Figure 6e). Subsequent cooling to the low temperature mesophase gave an obvious change to fan-shaped textures which are typical for Col_h phases (Figure 6f). The higher homologues of the dialkoxyphenyl series, **8** (C₁₂)₂ and **8** (C₁₄)₂, each showed only one broad liquid crystalline phase with temperature ranges of 85 K and 108 K respectively. POM investigations showed focal conic and broken fan-like textures with, especially for **8** (C₁₄)₂, large homeotropic areas, suggesting Col_h phases.

All members of the trisalkoxyphenyl series **8** (C_n)₃ with a minimum chain length of C₈ showed broad Col_h phases. The addition of a third side chain at the phenyl ring led to a further decrease of melting and clearing points as compared to the **8** (C_n)₂ series, while mesophase widths remained between 61 K and 121 K. For derivatives with longer alkyl chains (n = 10, 12, 14) stable room temperature Col_h phases were detected. The melting point of **8** (C₁₂)₃ was even below 0 °C at -15 °C, with a clearing point at 106 °C **8** (C₁₂)₃ showed the broadest mesophase (121 K) of all examined MIDA boronates. Under the POM fan-shaped textures of the Col_h phase revealed homeotropically aligned areas. Typical examples are shown for **8** (C₁₀)₃ (Figure 6g) and **8** (C₁₂)₃ (Figure 6h) respectively.

Crystal Structure

Fortunately, the non-mesomorphic MIDA boronate **8** (**C4**) provided single crystals suitable for X-ray crystal structure determination (Figure 7a).^[80] MIDA boronate **8** (**C4**) crystallized in the monoclinic centrosymmetric space group P21/c with one molecule in the asymmetric unit (full XRD data see Supporting Information). Crystal quality was only sufficient, indicated by a R(int) of 0.14, which is mainly caused by thermal fluctuations of the alkyl chains. In addition, the carbonyl function in the MIDA unit shows a slight rotational disorder with equivalent population factors (C3A=O3A / C3B=O3B). With respect to these conditions, the angles and distances at the boron and at the nitrogen are in good agreement with a tetrahedral surrounding. The angles at the boron are with values of O1-B1-O2 = 109.4(4)°, O1-B1-C6 = 113.0(5)° and O2-B1-C6 = 114.4(4)° close to the ideal tetrahedral angle. The same applies to the angles at the nitrogen atom, C4-N1-C5 = 111.1(5)°, C4-N1-C2 = 113.5(6)° and C5-N1-C2 = 108.5(5)°. The B-O distances are identical with 1.464(7) Å and 1.467(7) Å, respectively. The B-N distance is with a value of 1.658 Å in the same range as reported before for phenyl MIDA-boronate derivatives.⁸¹ The distance of the boron to the phenyl moiety is 1.573(7) Å. The packing diagram of the unit cell (Figure 7b) reveals a lamellar structure, in which polar and hydrophobic domains are formed by the MIDA boronate head groups and the alkoxy phenyl moieties, respectively. It should be emphasized that in the solid-state phenyl rings are involved in the interdigitated side chains. Thus, a polar MIDA boronate bilayer is sandwiched between two non-polar alkoxyphenyl bilayers, strongly resembling a smectic bilayer geometry.

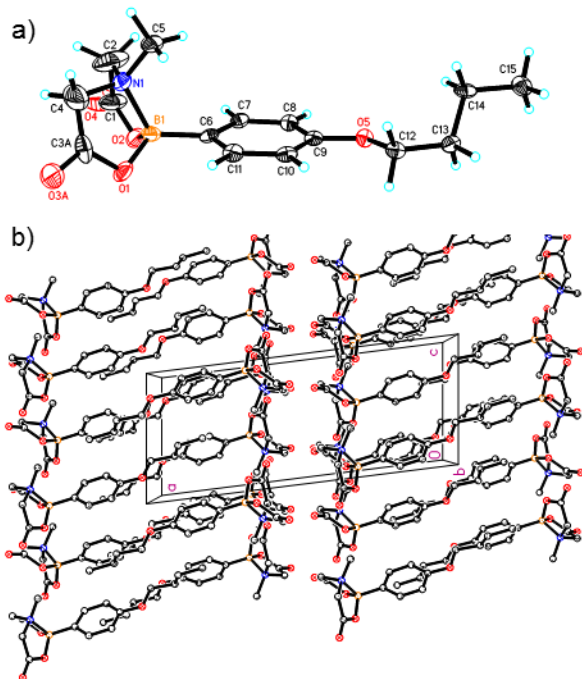


Figure 7. a) Molecular structure of **8** (**C4**) in the crystalline state. b) View of the unit cell along the b axis with distinct bilayer-like structure.

Quantum Chemical Calculations

As discussed in the previous section, the single crystal data of **8** (**C4**) gives an idea of how the molecules are arranged in the liquid-crystalline phase. With this information at hand, we wanted to understand the role of the MIDA head group. In particular, we wanted to investigate, whether there is any cross talk between the head group and the phenyl-alkoxy residues and understand the difference between MIDA boronates **8** and pinacol borolane **5**, boronic acids **6** and diethanolamine boronates **7** regarding phase behaviour.

The TURBOMOLE program package^[82,83] was employed for all quantum chemical calculations. Equilibrium structures were computed with Møller-Plesset second-order perturbation theory (MP2) and the def2-TZVPP basis sets for all atoms.^[84] The resolution-of-the-identity approach was used to speed up two-electron integral evaluations using the appropriate auxiliary basis sets.^[85,86] Relaxed MP2 electron densities were used for the natural population analysis (NPA)^[87] of the charge distribution and for computing dipole moments. As TURBOMOLE does not support computation of natural bond orbitals, we resorted to intrinsic bond orbitals (IBOs)^[88] based on the Hartree-Fock orbitals, which serve about the same purpose and for which an in-house

implementation is available. Graphical representations of the quantum chemical results were prepared with the TmoleX program.^[89]

The MP2 approach, in particular in connection with basis sets of triple- ζ type as used in this study, is known to give reliable structures for main group compounds with typical errors not exceeding 0.02 Å relative to highly accurate reference computations.^[90,91] We also note that the B-N bond distance computed with this approach is in much better agreement with the experimental value determined above for **8** (**C4**) as compared to density functional theory approaches. Details about this issue, further validation studies and the relevant parameters that characterize the bonding to the boron atom are given in the Supporting Information. All important structure parameters of the single crystal structure are well reproduced. Computed and experimental bond lengths agree within 0.02 Å, bond angles agree within 4 degrees. This confirms that the method describes the electronic structure of the molecules sufficiently well.

In order to shed further light on the bonding situation in the MIDA boronate head group, particularly around the boron atom, we computed the partial charges by a natural population analysis (NPA). The results are shown in Figure 8 (left).

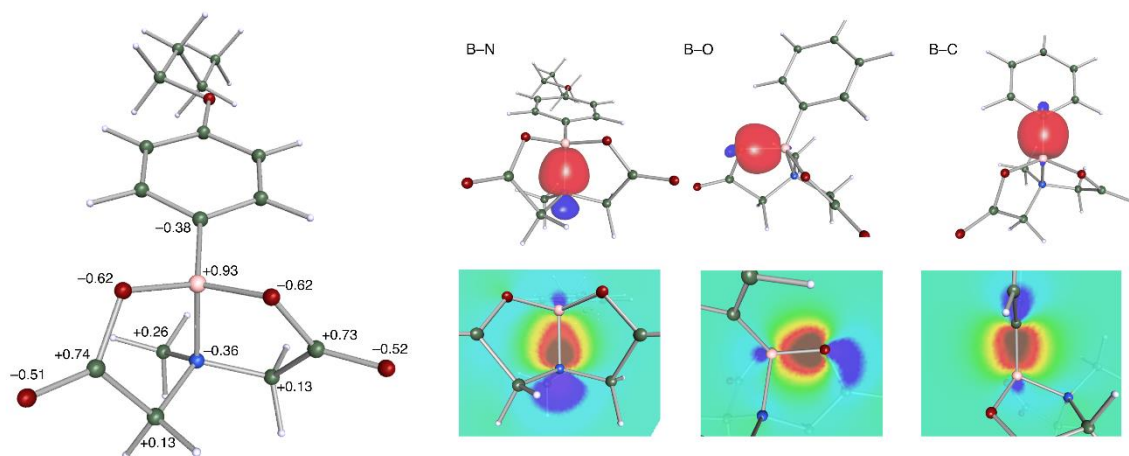


Figure 8. Left: Computed partial charges on the head group of **8**(**C4**). The charges refer to the indicated atoms or to CH₂ and CH₃ groups. Right: Intrinsic bond orbitals characterizing the bonding to boron. Isosurfaces are shown in the top row, while the bottom contains a color-coded contour plot in a plane containing boron and the corresponding neighboring atom.

According to the NPA, the boron atom is strongly charged with nearly one positive unit charge accumulated on this center. All surrounding atoms carry negative partial charges, indicating significantly polarized bonds to boron. This result clearly suggests to address the B–N bond as a dative bond (where the two electrons are still formally counted for nitrogen), as a Lewis-structure with a shared electron pair implies a negative formal charge on boron and a positive formal charge on nitrogen, clearly in contrast with the above result.

To further elucidate the bonding situation, we computed the intrinsic bond orbitals (IBOs) of the molecule. The orbitals representing the bonding to boron are shown in Figure 8 (right). The IBO corresponding to the B–N bond clearly shows strong nitrogen sp^3 character and little contribution from boron and should be thus addressed as a dative bond. The IBOs corresponding to the B–O and B–C bonds are also polarized but to a lesser degree. No further IBO indicating π -conjugation of the alkoxyphenyl ring and the MIDA boronate head-group is found.

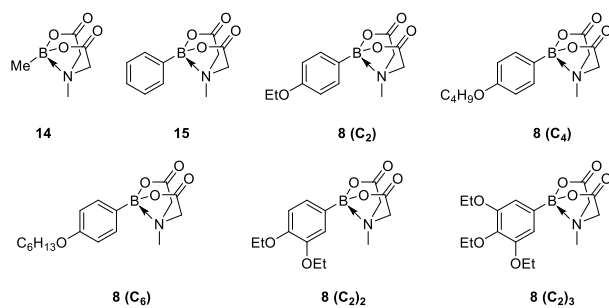


Figure 9. Derivatives computed for natural population analysis.

For closer investigation of the influence of the substituents the analysis of the partial charges was extended to seven different MIDA boronates carrying methyl (**14**), phenyl (**15**), 4-ethoxyphenyl (**8 (C₂)**), 4-butoxyphenyl (**8 (C₄)**), 4-hexyloxyphenyl (**8 (C₆)**), 3,4-diethoxyphenyl (**8 (C₂)₂**) and 3,4,5-triethoxyphenyl (**8 (C₂)₃**) units at the boron atom (Figure 9). This study revealed that the substituents have a negligible influence on the electronic structure of the MIDA boronate group. Neither the type of substituent in **14**, **15** and **8 (C₂)**, i.e. methyl vs. phenyl vs. 4-ethoxyphenyl nor the length of the side chains in **8 (C₂)**, **8 (C₄)**, and **8 (C₆)** or the number of side chains in **8 (C₂)**, **8 (C₂)₂** and **8 (C₂)₃** give a substantial difference of the partial charges. The partial charge on boron changes by less than $0.01 e$, for the remaining atoms by even less than $0.002 e$ (Table 1 and Supporting Information). We therefore conclude that the MIDA boronate head group is electronically fully decoupled from the residue at the boron atom.

Table 1. Comparison of computed partial charges of boron and its neighboring atoms.

Substituent	Compound	B1	N1	O1	O2	C6
methyl	14	+0.924	-0.361	-0.617	-0.618	-0.940 ^a
phenyl	15	+0.929	-0.356	-0.616	-0.618	-0.362
4-ethoxyphenyl	8(C₂)	+0.931	-0.357	-0.616	-0.618	-0.382
4-butoxyphenyl	8(C₄)	+0.931	-0.357	-0.616	-0.618	-0.382
4-hexyloxyphenyl	8(C₆)	+0.931	-0.357	-0.616	-0.618	-0.382
3,4-diethoxyphenyl	8(C₂)₂	+0.933	-0.357	-0.616	-0.617	-0.376
3,4,5-diethoxyphenyl	8(C₂)₃	+0.934	-0.357	-0.616	-0.619	-0.358

^aThe partial charge of the entire CH₃ group is -0.274 *e*.

This result was further supported by IR and Raman spectroscopic studies at room temperature (for details on the measuring conditions see Supporting Information). The following B-N stretching modes were observed in the IR and Raman spectra respectively: $\nu(\text{B-N}) = 592$ and 591 cm^{-1} for **8 (C₁₀)**, 587 and 589 cm^{-1} for **8 (C₁₀)₂**, 587 and 593 cm^{-1} for **8 (C₁₀)₃**. The values do not show any differences between mono-, di- and tri-substituted phenyl derivatives further supporting the absence of any electronic communication between the aryl ring and the B-N bond.

From the above theoretical and experimental data, we anticipated that the distinct mesomorphic behaviour of MIDA boronates **8** – as compared to structurally related boron compounds **5** – **7**, which carry the same aryl moiety – should be somehow related to the polar character of the head group. Therefore, the electronic properties of the MIDA group in the model system **8 (C₂)** were compared with the other boron containing groups: diethanolamine boronate **7 (C₂)**, boronic acid **6 (C₂)**, and pinacol borolane **5 (C₂)**. Note that our findings in Table 1 strongly suggested that we could confine our study to the ethoxy group (abbreviated as C₂), as the length of the alkyl chain did not have any significant influence on the electronic structure of the head group.

Our computations showed that the head groups of compounds **5** – **8** indeed have a significantly different polar character, see Figure 10. The strongly alternating partial charges on the MIDA boronate **8 (C₂)** as shown in Figure 8, already suggested that this group carries a strong dipole moment. This is in fact the case, we computed a dipole moment of 7.6 Debye units. More detailed insight is gained from inspecting the electrostatic potential of the molecule, Figure 10a. The oxygen atoms of the carboxyl groups accumulate negative charge and give rise to a strongly negative potential in this region. Positive charge is accumulated near the opposite methyl group and methylene bridges. As indicated in Figure 10a, the charge distribution can be qualitatively

addressed as originating from two distributed dipoles. As we will discuss below, this charge distribution may in fact rationalize the formation of a layered structure.

Replacing the carboxyl units in MIDA boronate **8** (C_2) by alkoxy groups in diethanolamine boronate **7** (C_2) resulted in a much less polar charge distribution (Figure 10b). The overall dipole moment is still 5.9 Debye units, but the negative charges accumulate in a much smaller area. Hence we do not get the distributed dipoles as discussed for **8** (C_2). The same is observed for boronic acid **6** (C_2) and pinacol borolane **5** (C_2) which also have much smaller dipole moments of 2.8 and 1.4 Debye units, respectively (Figure 10c,d).

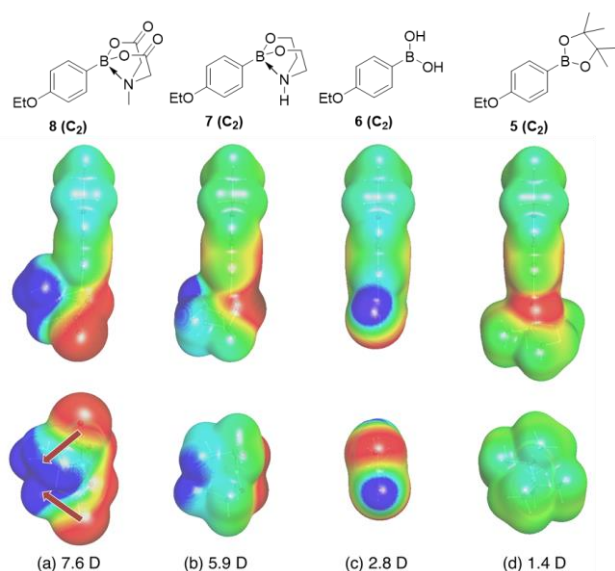


Figure 10. Visualization of the electrostatic potential of different boron containing head-groups in MIDA boronate **8** (C_2), diethanolamine boronate **7** (C_2), boronic acid **6** (C_2) and pinacol borolane **5** (C_2) with a 4-ethoxy-phenyl ring as further residue at the boron atom. The electrostatic potential is color coded (red = -1.9 eV to blue = $+1.9$ eV) on an isosurface of the electron density (0.0067 \AA^{-3}). Two different perspectives are shown (from the side and from below). Computed dipole moments are given on the bottom of each column. For (a) the electrostatic potential may be qualitatively described as originating from two distributed dipoles as indicated in the bottom view.

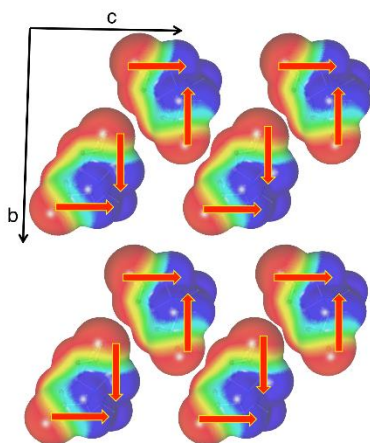


Figure 11. Schematic distribution of dipoles in the MIDA boronate packing scheme according to crystal structure of **8** (C_4).

As indicated above, the charge distribution computed for **8** (C_4) can be interpreted as two distributed dipoles. This charge distribution is compatible with a 2D packing of the molecules as derived from the crystal structure of **8** (C_4), see Figure 11. Note that cofacially arranged dipoles prefer an antiparallel alignment while dipoles arranged in a linear chain prefer parallel alignment.

The schematic distribution of the dipoles in Figure 11 also gives a hint on the mechanisms of the mesophase formation from MIDA boronates **8**. On the one hand, the different polarities of the MIDA and the alkoxyphenyl group lead to phase separation and formation of the bilayer structure. On the other hand, the strong dipolar interactions of the MIDA groups stabilizes the sublayer as shown in Figure 11, whereby a layer-like mesophase can be formed. In the case of **5**, **6**, and **7** either weaker tendencies of phase separation or weaker dipolar interactions do not support a stable bilayer structure. With the results of the quantum chemical calculations in hand it was possible to deduce a general understanding on the mesophase formation of the MIDA boronates **8** which was utilized to explain the following X-ray investigations.

Mesophase Geometries

To gain further insight in the phase geometries of the liquid crystalline MIDA boronates small (SAXS) and wide angle (WAXS) X-ray scattering experiments were conducted (for full XRD data see Supporting Information). First, the derivatives for which the POM investigations suggested a

layer-like mesophase were investigated. Therefore, the samples were investigated via SAXS at different temperatures during cooling from the isotropic liquid. From the obtained (001) XRD reflexes the respective layer spacings d were determined. In Figure 12a the results of monoalkoxyphenyl derivative **8** (**C10**) and bisalkoxyphenyl derivative **8** (**C10**)₂, in the high temperature mesophase, are depicted. During cooling the layer spacing gradually increased, which is typical for SmA mesophases, presumably because of a decreasing interdigitation of the alkoxy chains.^[92] Interestingly, the layer spacing of **8** (**C10**) is larger than that of **8** (**C10**)₂ although the latter has two side chains which should require more space than the one of the mono substituted derivative.

For better comparison, the layer spacings at the reduced clearing point d_{red} (at $0.95 \times T_c$)^[92] were calculated for all derivatives **8** (**C_n**) ($n = 6 - 14$) and **8** (**C_n**)₂ ($n = 6 - 10$) using the equations of the trendlines of the respective SAXS layer spacing temperature dependency. Additionally, for each compound the molecular lengths L (and $2L$) between the outer most atoms in the stretched *all-trans* conformation were calculated by using the Avogadro 1.1.1 software (Figure 12b).^[93] The d_{red} values for both substitution patterns **8** (**C_n**) and **8** (**C_n**)₂, and for **13** (**C12**) are between L and $2L$ indicating the formation of smectic bilayers SmA₂ for both series. However, the observed layer spacings differ increasingly with longer alkyl chains from the calculated bilayer distances indicating a stronger interdigitation with increasing alkyl chain lengths. Therefore, a comparison of the d_{red} values with the maximal interdigitated bilayers is of interest. The size of the MIDA boronate head group together with the attached phenyl ring is $L_{core} = 8.15 \text{ \AA}$. For maximum interdigitation it is assumed that the layer spacing is $L_{max} = L + L_{core}$, since the alkoxy side chains are completely interleaved (Fig. 12c). The values of L_{max} are very close to those of the respective layer spacings d_{red} indicating a strong interdigitation especially for longer chain lengths. For **8** (**C12**), **8** (**C14**), **13** (**C12**), and **8** (**C10**)₂ the calculated interdigitation give values of 99 %, indicating a complete interdigitation at the reduced clearing point. However, these findings do not suggest the participation of the core structure in the interdigitation as implied in the single crystal structure of **8** (**C4**) (Fig. 7b).

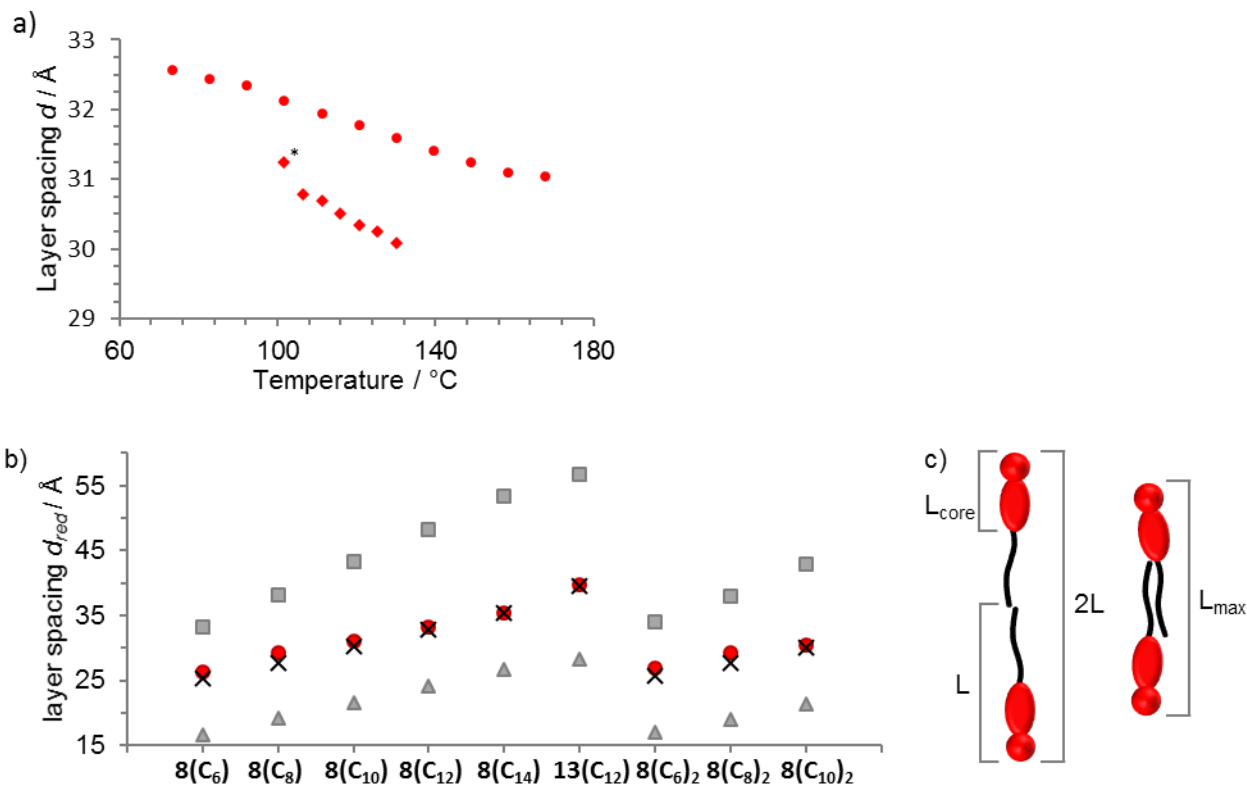


Figure 12. a) Layer spacing temperature dependency of \bullet $8(C_{10})$ and \blacksquare $8(C_{10})_2$ in the SmA_2 phase derived from SAXS experiments (* transition from the SmA_2 phase to the low temperature Col_h phase), b) layer spacing at reduced clearing points \bullet d_{red} compared to single (\blacktriangle , L) and double (\blacksquare , $2L$) molecular lengths, and to maximal interdigitation (\blacktimes , L_{max}), c) illustration of the molecular dimensions.

According to the DSC and POM studies (Figure 4c, Figure 6e,f) bisdecyloxy-substituted derivative $8(C_{10})_2$ displayed a second mesophase at lower temperatures in addition to the SmA_2 phase. The results of the XRD experiments of this lower temperature mesophase are shown in Figure 13a. The SAXS profile only displays one reflection indexed as (10) which is not sufficient for the assignment of the phase. However, the Col_h phase geometry was confirmed by the WAXS experiment shown in the inset of Figure 13a. In addition to the broad halo at 4.5 Å caused by the molten alkyl chains, a hexagonal orientation of the (10) reflection was detected, which is typical for Col_h mesophases.

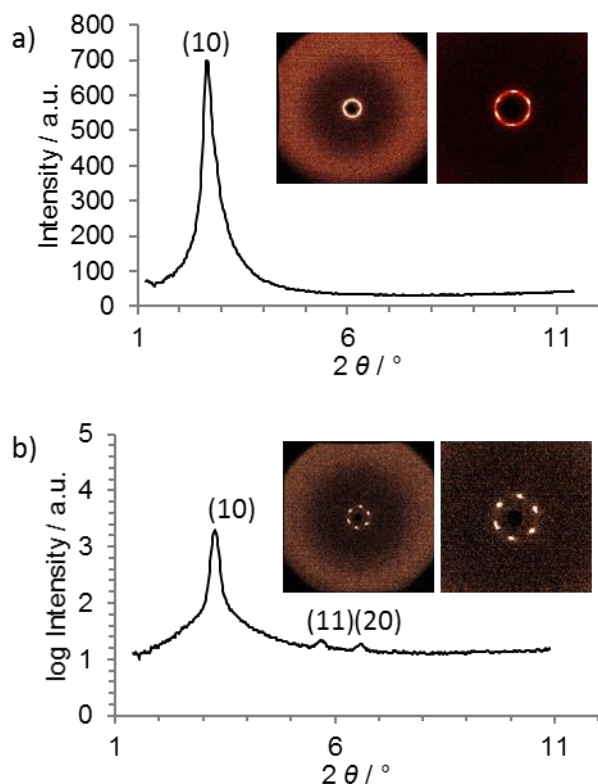


Figure 13. a) SAXS profile of **8** (C_{10})₂ at 90 °C and WAXS diffraction pattern at 90 °C (left), magnification of inner signals of the WAXS pattern (right), b) SAXS profile of **8** (C_8)₃ at 90 °C and WAXS diffraction pattern at 90 °C (left), magnification of inner signals of the WAXS pattern (right).

For the remaining dialkoxy- and trialkoxyphenyl MIDA boronates **8** (C_n)₂ ($n = 12, 14$) and **8** (C_n)₃ ($n = 8 - 14$) XRD investigations confirmed the assignment of Col_h phase geometries. For derivatives **8** (C_{14})₂, **8** (C_8)₃, and **8** (C_{10})₃ hexagonal orientations of the (10) reflection were found either in the WAXS or SAXS experiments. Figure 13b shows the results of the XRD experiments for **8** (C_8)₃. The SAXS profile displays three reflexes in the ratio of $1 : 1/\sqrt{3} : 1/2$ indexed as (10), (11), and (20).^[94] Moreover, the depicted WAXS pattern displays a halo in the wide angle region and six distinct reflexes in the small angle region arranged in a hexagonal manner supporting the assignment of the Col_h phase.

In order to rationalize the transition from the smectic mesophases observed for mono- **8** (C_n) ($n = 6 - 14$) and dialkoxy-substituted derivatives **8** (C_n)₂ ($n = 6 - 10$) to columnar hexagonal mesophases for **8** (C_n)₂ ($n = 10 - 14$) and trialkoxy-substituted MIDA boronates **8** (C_n)₃ ($n = 8 - 14$) minimization of free volume and increasing sterical demand of the alkyl chains seem to govern

mesophase formation. Presumably for one or two side chains a lamellar organization is preferred resulting in SmA₂ bilayers (Figure 14). However, as the lengths of the two alkoxy chains exceed C₁₀ or an additional third chain is attached to the phenyl ring, the bilayer cannot accommodate any longer the MIDA boronates **8** (C_n)_m in an anti-parallel interdigitated fashion, but a micellar-like aggregate of the wedge-shaped mesogens is favoured, resulting in the Col_h phase. The number of molecules per disk Z could be calculated according to $Z = \frac{\rho \cdot N_A \cdot A \cdot h}{M}$, where ρ is the density (considered close to 1), N_A is Avogadro's constant, A is the columnar cross section, h is the height of a disc (approximately the d -value of the respective halo), and M is the molecular weight of a single molecule.^[95]

The results of these calculations are summarized in Table 2. For **8** (C₁₀)₂, a Z -value of 6 was calculated. Therefore, in a hexagonal lattice with a lattice parameter $a_{hex} = 38.3 \text{ \AA}$ one disc consists of 6 molecules forming a micellar-like aggregate. Upon increase of the side chain lengths to $n = 12$ and $n = 14$ respectively, the lattice parameters remained relatively constant at $a_{hex} = 37.7 \text{ \AA}$ and $a_{hex} = 38.3 \text{ \AA}$ respectively, while the number of molecules per disc decreased to $Z = 5$ for **8** (C₁₂)₂ and **8** (C₁₄)₂, presumably due to increased interdigitation and increased volume requirements of a single molecule within the micellar aggregate. For the trisalkoxy-substituted MIDA boronate **8** (C₈)₃ with C₈ chains a lattice parameter $a_{hex} = 31.2 \text{ \AA}$ was obtained and the calculated Z -value was 4. Upon increasing the side chain lengths to $n = 10$ and $n = 12$, the lattice parameters increased steadily to $a_{hex} = 33.5 \text{ \AA}$ and $a_{hex} = 36.3 \text{ \AA}$ respectively, while the calculated Z -values remained constant at $Z = 4$. Probably due to the increased volume fraction of the trisubstituted MIDA boronates, e.g. **8** (C₁₂)₃ as compared to the corresponding disubstituted counterpart **8** (C₁₂)₂ fewer molecules can be accommodated in the micellar aggregate, thus the Z -value decreases from 6 and 5 in the disubstituted series to 4 in the trisubstituted series. However, constant Z -values for **8** (C₈)₃, **8** (C₁₀)₃ and **8** (C₁₂)₃ are only possible, if the lattice parameter increases with increasing chain lengths. Surprisingly, in case of MIDA boronate **8** (C₁₄)₃ with three C₁₄ chains a significantly larger lattice parameter of $a_{hex} = 50.1 \text{ \AA}$ was detected. In order to accommodate such a lattice, the number of molecules with the micellar aggregate needs to be increased considerably from $Z = 4$ to $Z = 7$.

Table 2. XRD data for MIDA boronates displaying hexagonal columnar mesophases **8** (**C**₁₀)₂ – **8** (**C**₁₄)₂ and **8** (**C**₈)₃ – **8** (**C**₁₄)₃.

Mesophase	$a_{\text{hex}}^a / \text{Å}$	$d_{\text{exp}} (d_{\text{calc}}) / \text{Å}$	hk	Z^b	
8 (C ₁₀) ₂	Col _h at 90 °C	$a = 38.3$	33.1	(10)	6
	<i>p6mm</i>		4.5	halo	
8 (C ₁₂) ₂	Col _h at 120 °C	$a = 37.7$	32.6	(10)	5
	<i>p6mm</i>		16.3 (16.31)	(20)	
				4.1	halo
8 (C ₁₄) ₂	Col _h at 140 °C	$a = 38.3$	33.2	(10)	5
	<i>p6mm</i>		4.6	halo	
8 (C ₈) ₃	Col _h at 90 °C	$a = 31.2$	27.0	(10)	4
	<i>p6mm</i>		15.6 (15.60)	(11)	
			13.4 (13.51)	(20)	
			4.2	halo	
8 (C ₁₀) ₃	Col _h at 90 °C	$a = 33.5$	29.0	(10)	4
	<i>p6mm</i>		4.6	halo	
8 (C ₁₂) ₃	Col _h at 70 °C	$a = 36.3$	31.5	(10)	4
	<i>p6mm</i>		4.7	halo	
8 (C ₁₄) ₃	Col _h at 60 °C	$a = 50.1$	43.4	(10)	7
	<i>p6mm</i>		21.7 (21.71)	(20)	
			14.4 (14.47)	(30)	
			10.1 (9.96)	(32)	
			9.5 (9.48)	(41)	
			8.8 (8.68)	(50)	
	4.7	halo			

^a The parameter a_{hex} corresponds to the column diameter and was calculated with $a_{\text{hex}} = 2 \cdot d_{10} / \sqrt{3}$. ^b Rounded to integers.^[95]

The X-ray diffraction data together with the observation, that even MIDA boronates with relatively short alkyl chains, i.e. C₆ for **8** (**C**_n), **8** (**C**_n)₂ and C₈ for **8** (**C**_n)₃ displayed mesomorphic properties suggested that the dipolar interactions between the MIDA boronate head groups play an important role in the stabilization of the mesophase, even in the absence of either strong van der Waals interactions exerted by long alkoxy chains or strong π – π -interactions.

Accepted Manuscript

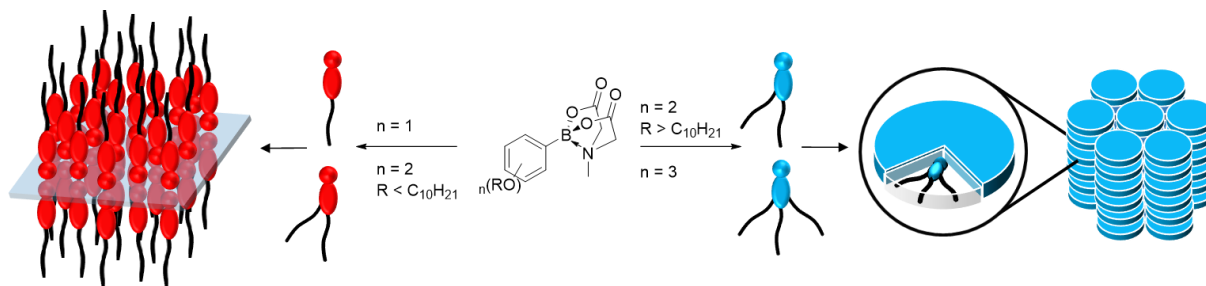


Figure 14. Proposed self-assembly of the MIDA boronates **8** into SmA_2 or Col_h mesophases depending on the number and lengths of the alkoxy side chains.

Conclusion

In conclusion, we have demonstrated for the first time that MIDA boronates can indeed induce thermotropic liquid crystalline properties even when the MIDA boronate head group is connected to a mono-, di- or trialkoxyphenyl unit with relatively short alkyl chain lengths of C_6 for **8** (C_n), **8** (C_n)₂ or C_8 for **8** (C_n)₃. In order to understand, why MIDA boronates **8** form stable mesophases, whereas the corresponding pinacol borolanes **5**, boronic acid **6** or diethylamino boronates **7** are devoid of any liquid crystalline self-assembly, quantum chemical calculations were carried out. The calculations clearly revealed a charge distribution at the B-N bond, where the positive charge is located at the boron atom, while the negative charge is positioned at the nitrogen atom, suggesting that the bonding situation in the MIDA boronate should be characterized by a dative bond rather than a zwitterionic Lewis structure. According to the calculations the MIDA head group is electronically fully decoupled from the remaining substituent at the boron, regardless whether the phenyl ring carries ethoxy substituents or longer alkoxy chains. This allowed us to use non-mesomorphic 4-ethoxyphenyl MIDA boronate **8** (C_2) as a mimic for higher homologues **8** (C_n) ($n \geq 6$) capable of liquid crystalline self-assembly in subsequent calculations, where the unique properties of the MIDA head group in comparison with diethylamino boronate, boronic acid and pinacol borolane head group were assessed. According to the calculations the overall dipole moment decreases in the series **8** (C_2) > **7** (C_2) > **6** (C_2) > **5** (C_2), suggesting that dipolar interactions between mono-alkoxy-substituted MIDA boronates **8** (C_n) play a prominent role in the stabilization of smectic mesophases. Dipolar interactions even seem to overrule hydrophobic interactions or hydrogen bonds which are present in the boronic acid derivatives **5** (C_n) - **7** (C_n). Experimental results showed that for MIDA boronates **8** (C_n)_m the mesophase type is determined by the number and lengths of alkoxy chains, i.e. for one or two short alkoxy chains smectic A

phases were observed, while two longer or three alkoxy chains led to hexagonal columnar mesophases. Thus, the scope of MIDA boronates has been extended far beyond cross-coupling reagents into tailor-made soft matter. It should be emphasized that our work on dipolar interactions in liquid crystalline MIDA boronates complement recent studies by Kaszynski,^[96] who was able to quantify the contribution of dipolar interactions to the clearing temperature of carborane clusters via isosteric and isoelectronic replacement. Future work must demonstrate, whether dipolar interactions can be employed to generate other novel thermotropic materials.

Acknowledgement

Generous financial support by the Deutsche Forschungsgemeinschaft, the Ministerium für Wissenschaft, Forschung und Kunst des Landes Baden-Württemberg and the Bundesministerium für Bildung und Forschung is gratefully acknowledged.

References

- [1] Review: Z. Liu, T. B. Marder, *Angew. Chem. Int. Ed.* **2008**, *47*, 242.
- [2] Review: G. Vancoille, R. Hoogenboom, *Polymer Chem.* **2016**, *7*, 5484.
- [3] Review: Y. Weng, X. Wang, X. Wang, Y. Bando, D. Golberg, *Chem. Soc. Rev.* **2016**, *45*, 3989.
- [4] Review: C. D. Entwistle, T. B. Marder, *Angew. Chem. Int. Ed.* **2002**, *41*, 2927.
- [5] Review: D. Bonifazi, F. Fasano, M. Mercedes Lorenzo-Garcia, D. Marinelli, H. Oubaha, J. Tasseroul, *Chem. Comm.* **2015**, *51*, 15222.
- [6] Review: T. Tanaka, Y. Chujo, *Macromol. Rapid Commun.* **2012**, *33*, 1235.
- [7] Review: T. B. Marder, *Science* **2006**, *314*, 69.
- [8] I. Sanchez; C. Nunez, J. A. Campo, M. R. Torres, M. Cano, C. Lodeiro, *J. Mater. Chem. C* **2014**, *2*, 9653.
- [9] Y. Bando, T. Sakurai, S. Seki, H. Maeda, *Chem. Asian J.* **2013**, *8*, 2088.
- [10] Y. Terashima, M. Takayama, K. Isozaki, H. Maeda, *Chem. Commun.* **2013**, *49*, 2506.
- [11] M. J. Mayoral, P. Ovejero, J. A. Campo, J. V. Heras, E. Oliveira, B. Pedras C. Lodeiro, M. Cano, *J. Mater. Chem.* **2011**, *21*, 1255.
- [12] I. Sanchez, M. J. Mayoral, P. Ovejero, J. A. Campo, J. V. Heras, M. Cano, C. Lodeiro, *New J. Chem.* **2010**, *34*, 2937.
- [13] O. A. Turanova, E. V. Kaledyaeva, O. I. Gnezdilov, S. I. Nikitin, A. N. Turanov, *Russ. J. General Chem.* **2010**, *80*, 258.

- [14] O. A. Turanova, A. N. Turanov, D. V. Lapaev, O. I. Gnezdilov, S. V. Lobkov, Y. G. Gayametdinov, *Russ. J. General Chem.* **2006**, *76*, 730.
- [15] S. Mula, S. Frein, V. Russo, G. Ulrich, R. Ziessel, J. Barbera, R. Descheneaux, *Chem. Mater.* **2015**, *27*, 2332.
- [16] H. Gopee, X. Kong, Z. He, I. Chambrier, E. L. Hughes, G. J. Tizzard, S. J. Coles, A. N. Cammidge, *J. Org. Chem.* **2013**, *78*, 9505.
- [17] A. Florian, M. J. Mayoral, V. Stepanenko, G. Fernandez, *Chem. Eur. J.* **2012**, *18*, 14957.
- [18] J.-H. Olivier, J. Barbera, E. Bahaidarah, A. Harriman, R. Ziessel, *J. Am. Chem. Soc.* **2012**, *134*, 6100.
- [19] M. Benstead, G. A. Rosser, A. Beeby, G. H. Mehl, R. W. Boyle, *New J. Chem.* **2011**, *35*, 1410.
- [20] M. Benstead, G. A. Rosser, A. Beeby, G. H. Mehl, R. Boyle, *Photochem. Photobiol. Sci.* **2011**, *10*, 992.
- [21] J.-H. Olivier, F. Camerel, G. Ulrich, J. Barbera, R. Ziesse *Chem. Eur. J.* **2010**, *16*, 7134.
- [22] S. Frein, F. Camerel, R. Ziessel, J. Barbera, R. Descheneaux, *Chem. Mater.* **2009**, *21*, 3950.
- [23] F. Camerel, G. Ulrich, J. Barbera, R. Ziessel, *Chem. Eur. J.* **2007**, *13*, 2189.
- [24] E. Cavero, D. P. Lydon, S. Uriel, M. R. de la Fuente, J. L. Serrano, R. Gimenez, *Angew. Chem. Int. Ed.* **2007**, *46*, 5175.
- [25] E. Cavero, M. R. de la Fuente, E. Beltran, P. Romero, J. L. Serrano, R. Gimenez, *Chem. Mater.* **2007**, *19*, 6230.
- [26] F. Camerel, L. Bonardi, G. Ulrich, L. Charbonniere, B. Donnio, C. Borgogne, D. Guillon, *Chem. Mater.* **2006**, *18*, 5009.
- [27] F. Camerel, L. Bonardi, M. Schmutz, R. Ziessel, *J. Am. Chem. Soc.* **2006**, *128*, 4548.
- [28] B. Ringstrand, P. Kaszynski, *Acc. Chem. Res.* **2013**, 214.
- [29] B. Ringstrand, *Liq. Cryst. Today* **2013**, *22*, 22.
- [30] B. P. Dash, R. Satapathy, J. A. Maguire, N. A. Hosmane, *New J. Chem.* **2011**, *35*, 1955.
- [31] B. Ringstrand, P. Kaszynski, *J. Mater. Chem.* **2011**, *21*, 90.
- [32] B. Ringstrand, P. Kaszynski, *J. Mater. Chem.* **2010**, *20*, 9613.
- [33] M. Nieuwenhuyzen, K. R. Seddon, F. Teixidor, A. V. Puga, C. Vinas, *Inorg. Chem.* **2009**, *48*, 889.
- [34] M. Jasinski, A. Jankowiak, A. Januszko, M. Bremer, D. Pauluth, P. Kaszynski, *Liq. Cryst.* **2008**, *35*, 343.
- [35] P. Kaszynski, J. Huang, G. S. Jenkins, K. A. Bairamov, D. Lipiak, *Mol. Cryst. Liq. Cryst. A* **1995**, *260*, 315.

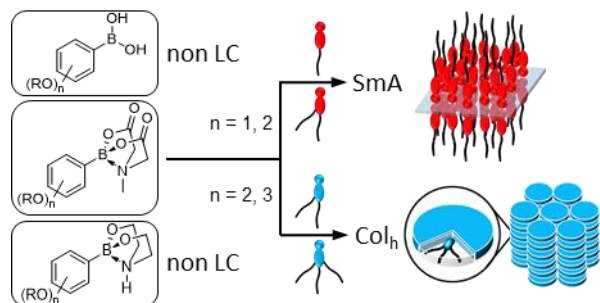
- [36] J. Pecyna, P. Kaszynski, B. Ringstrand, M. Bremer, *J. Mater. Chem. C* **2014**, *2*, 2956.
- [37] J. Pecyna, D. Pocięcka, P. Kaszynski, *J. Mater. Chem. C* **2014**, *2*, 1585.
- [38] B. Ringstrand, H. Monoku, P. Kaszynski, *J. Mater. Chem.* **2009**, *19*, 4805.
- [39] V. Coeffard, X. Moreau, C. Thomassigny, C. Greck, *Angew. Chem.* **2013**, *125*, 5794.
- [40] A. Suzuki, *Angew. Chem. Int. Ed.* **2011**, *50*, 6722.
- [41] N. Miyaura, *N. Bull. Chem. Soc. Jpn.* **2008**, *81*, 1535.
- [42] N. Miyaura, *Topics Curr. Chem.* **2002**, *219*, 11.
- [43] K. Seto, S. Takahashi, T. Takara, *J. Chem. Soc., Chem. Commun.* **1985**, 122.
- [44] K. Seto, H. Matsubara, S. Takahashi, M. Murakami, S. Miyake, T. Masumi, T. Ando, A. Fukami, *J. Chem. Soc., Chem. Commun.* **1988**, 56.
- [45] M. Murakami, S. Miyake, T. Masumi, T. Ando, A. Fukami, S. Takahashi, K. Seto, T. Takara, *Mol. Cryst. Liq. Cryst.* **1988**, *162B*, 149.
- [46] H. Matsubara, K. Seto, H. Tabushi, H. Imazaki, S. Takahashi, *Chem. Lett.* **1989**, 1519.
- [47] H. Matsubara, K. Seto, S. Takahashi, *S. Mol. Cryst. Liq. Cryst. A* **1994**, *241*, 9.
- [48] L. A. Tatum, C. J. Johnson, A. A. P. Fernando, B. C. Ruch, K. K. Barakoti, M. A. Alpuche-Aviles, B. T. King, *Chem. Sci.* **2012**, *3*, 3261.
- [49] T. Wöhrle, A. Baro, S. Laschat, *Materials* **2014**, *7*, 4045.
- [50] M. Belloni, M. Manickam, Z.-H. Wang, J. A. Preece, *Mol. Cryst. Liq. Cryst.* **2003**, *399*, 93.
- [51] T. Yasuda, T. Shimizu, F. Liu, G. Ungar, T. Kato, *J. Am. Chem. Soc.* **2011**, *133*, 13437.
- [52] T. Wöhrle, J. Kirres, M. Kaller, M. Mansueto, S. Tussetschläger, S. Laschat, *J. Org. Chem.* **2014**, *79*, 10143.
- [53] Y. Wang, Y. Liu, J. Luo, H. Qi, X. Li, M. Nin, M. Liu, D. Shi, W. Zhu, Y. Cao, *Dalton Trans.* **2011**, *40*, 5046.
- [54] T. Wöhrle, S. J. Beardsworth, C. Schilling, A. Baro, F. Giesselmann, S. Laschat, *Soft Matter* **2016**, *12*, 3730.
- [55] M. Belloni, M. Manickam, P. R. Ashton, B. M. Kariuki, J. A. Preece, N. Spencer, J. Wilkie, *Mol. Cryst. Liq. Cryst.* **2001**, *369*, 17.
- [56] C. Sauer, S. Diele, N. Lindner, C. Tschierske, *Liq. Cryst.* **1998**, *25*, 109.
- [57] R. Contreras, T. Mancilla, *J. Organomet. Chem.* **1986**, *307*, 1.
- [58] N. Farfán, T. Mancilla, D. Castillo, G. Uribe, L. Carrillo, P. Joseph-Nathan, R. Contreras, *J. Organomet. Chem.* **1990**, *381*, 1.
- [59] E. P. Gillis, M. D. Burke, *J. Am. Chem. Soc.* **2007**, *129*, 6716.

- [60] J. Li, A. S. Grillo, M. D. Burke, *Acc. Chem. Res.* **2015**, *48*, 2297.
- [61] D. N. Reinemann, A. M. Wright, J. D. Wolfe, G. S. Tschumper, N. I. Hammer, *J. Phys. Chem. A* **2011**, *115*, 6426.
- [62] a) C. Tschierske, in *Handbook of Liquid Crystals*, J. W. Goodby, P. J. Collings, T. Kato, C. Tschierske, H. F. Gleeson, P. Raynes, (eds.), 2nd ed., Wiley-VCH: Weinheim, **2014**; vol. 5, pp. 45. b) C. Tschierske, *ibid*, vol. 5, pp. 1. c) C. Tschierske, *Angew. Chem. Int. Ed.* **2013**, *52*, 8828. d) C. Tschierske, *Isr. J. Chem.* **2012**, *52*, 935.
- [63] J. W. Goodby, E. J. Davies, R. J. Mandle, S. J. Cowling, in *Handbook of Liquid Crystals*, J. W. Goodby, P. J. Collings, T. Kato, C. Tschierske, H. F. Gleeson, P. Raynes, (eds.), 2nd ed., Wiley-VCH: Weinheim, **2014**; vol. 1, pp. 231.
- [64] J. W. Goodby, R. J. Mandle, E. J. Davis, T. Zhong, S. Cowling, *Liq. Cryst.* **2015**, *42*, 593.
- [65] D. Chen, M. R. Tuchband, B. Horanyi, E. Korblova, D. M. Walba, M. A. Glaser, J. E. MacLennan, N. A. Clark, *Nature Comm.* **2015**, *6*, 7763.
- [66] K. V. Axenov, S. Laschat, *Materials* **2011**, *4*, 206.
- [67] M. Mansueto, S. Laschat, in *Handbook of Liquid Crystals*, J. W. Goodby, P. J. Collings, T. Kato, C. Tschierske, H. F. Gleeson, P. Raynes, (eds.), 2nd ed., Wiley-VCH: Weinheim, **2014**; vol. 6, pp. 231.
- [68] S. Chen, S. H. Eichhorn, *Isr. J. Chem.* **2012**, *52*, 830.
- [69] L. Douce, J.-M. Suisse, D. Guillon, A. Taubert, *Liq. Cryst.* **2011**, *38*, 1653.
- [70] a) K. Goossens, K. Lava, C. W. Bielawski, K. Binnemans, *Chem. Rev.* **2016**, *116*, 4643. b) K. Binnemans, *Chem. Rev.* **2005**, *105*, 4148.
- [71] A. Martinez-Felipe, C. T. Imrie, *J. Mol. Struct.* **2015**, *1100*, 429.
- [72] S. Fujimura, Y. Yamamura, M. Hishida, S. Nagatomo, K. Saito, *Liq. Cryst.* **2014**, *41*, 927.
- [73] a) M. A. Osipov, G. Pajak, *Liq. Cryst.* **2016**, doi: 10.1080/02678292.2016.1247474. b) G. Pajak, M. A. Osipov, *Phys. Rev. E* **2013**, *88*, 012507.
- [74] a) K. Saito, M. Hishida, Y. Yamamura, *Soft Matter* **2015**, *11*, 8493. b) K. Horiuchi, Y. Yamamura, R. Pelka, M. Sumita, S. Yasuzuka, M. Massalska-Arodz, K. Saito, *J. Phys. Chem. B* **2010**, *114*, 4870. c) Y. Yamamura, T. Adachi, T. Miyazawa, K. Horiuchi, M. Sumita, M. Massalska-Arodz, S. Urban, K. Saito, *J. Phys. Chem. B* **2012**, *116*, 9255. d) T. Miyazawa, Y. Yamamura, M. Hishida, S. Nagatomo, M. Massalska-Arodz, K. Saito, *J. Phys. Chem. B* **2013**, *117*, 8293.
- [75] Review on lyotropic liquid crystals: C. Fong, T. Le, J. Drummond, *Chem. Soc. Rev.* **2012**, *41*, 1297.
- [76] K. Sadakane, H. Seto, M. Nagao, *Chem. Phys. Lett.* **2006**, *426*, 61.

- [77] Y. Yamaoka, Y. Taniguchi, S. Yasuzuka, Y. Yamamura, K. Saito, *J. Chem. Phys.* **2011**, *135*, 044705.
- [78] C. M. Gordon, J. D. Holbrey, A. R. Kennedy, K. R. Seddon, *J. Mater. Chem.* **1998**, *8*, 2627.
- [79] S. G. Ballmer, E. P. Gillis, M. D. Burke, *Org. Synth.* **2009**, *86*, 344.
- [80] CCDC-1486006 contains the supplementary crystallographic information for **8 (C4)**. The data can be obtained free of charge from The Cambridge Crystallographic Data Center via <https://summary.ccdc.cam.ac.uk/structure-summary-form>.
- [81] T. M. Percino, R. M. F. Ancona, M. L. Martínez, *Polyhedron* **2009**, *28*, 2771.
- [82] TURBOMOLE V7.0.1 2015, a development of University of Karlsruhe and Forschungszentrum Karlsruhe GmbH, 1989-2007, TURBOMOLE GmbH, since 2007; available from <http://www.turbomole.com>.
- [83] F. Furche, R. Ahlrichs, C. Hättig, C. Klopper, M. Sierka, F. Weigend, *Comput. Mol. Sci.* **2013**, *4*, 91.
- [84] F. Weigend, R. Ahlrichs *Phys. Chem. Chem. Phys.* **2005**, *7*, 3297.
- [85] F. Weigend, M. Häser, *Theor. Chem. Acc.* **1997**, *97*, 331.
- [86] F. Weigend, M. Häser, H. Patzelt, R. Ahlrichs, *Chem. Phys. Lett.* **1998**, *294*, 143.
- [87] A. Reed, R. Weinstock, F. Weinhold, *J. Chem. Phys.* **1985**, *83*, 735.
- [88] G. Knizia, *J. Chem. Theory. Comput.* **2013**, *9*, 4834.
- [89] C. Steffen, K. Thomas, U. Huniar, A. Hellweg, O. Rubner, A. Schroer, *J. Comput. Chem.* **2010**, *31*, 2967.
- [90] K.L. Bak, J. Gauss, P. Jørgensen, J. Olsen, T. Helgaker, and J.F. Stanton, *J. Chem. Phys.* **2001**, *114*, 6548.
- [91] I. S. Coriani, D. Marchesan, J. Gauss, C. Hättig, T. Helgaker, and P. Jørgensen, *J. Chem. Phys.* **2005**, *123*, 184107.
- [92] P. H. J. Kouwer, T. M. Swager, T. M. *J. Am. Chem. Soc.* **2007**, *129*, 14042.
- [93] Avogadro: an open-source molecular builder and visualization tool. Version 1.1.1. M. D. Hanwell, D. E. Curtis, D. C. Lonie, T. Vandermeersch, E. Zurek, G. R. J. Hutchison, *Cheminformatics* **2012**, *4*, 17.
- [94] S. K. Prasad, D. S. S. Rao, S. Chandrasekhar, S. Kumar, *Mol. Cryst. Liqui. Cryst.* **2003**, *396*, 121.
- [95] M. Lehmann, C. Köhn, H. Meier, S. Renker, A. Oehlhof, *J. Mater. Chem.* **2006**, *16*, 441.
- [96] A. Jankowiak, A. Sivaramamoorthy, D. Pocięcha, P. Kaszynski, *RSC Adv.* **2014**, *4*, 53907.

Accepted Manuscript

Table of Contents



In contrast to the non-mesomorphic aryl boronic acids and diethanolamine boronates, MIDA boronates form smectic or columnar mesophases which was rationalized by strong dipolar interactions according to quantum chemical calculations.